Available online at www.eccomasproceedia.org
Eccomas Proceedia COMPDYN (2023) 143-157

ECCOMAS
Proceedia

COMPDYN 2023
9th ECCOMAS Thematic Conference on
Computational Methods in Structural Dynamics and Earthquake Engineering
M. Papadrakakis, M. Fragiadakis (eds.)
Athens, Greece, 12-14 June 2023

REDESIGNING THE TRANSITION PIECE FOR MITIGATING THE SEISMIC RESPONSE OF OFFSHORE WIND TURBINES

Rohollah Rostami[1], **Alessandro Tombari**[1]

[1] University of Brighton

University of Brighton, Cockcroft Building, Lewes Road, Brighton, BN2 4GJ, United Kingdom
R.Rostami@Brighton.ac.uk, A.Tombari@Brighton.ac.uk

Abstract

Wind turbines are slender and light-damped structures which make them susceptible to earthquake-induced vibrations. Because of the current expansion into new markets, where taller and larger turbines will be constructed in earthquake-prone areas, seismic design cannot be anymore overlooked. In certain regions, earthquake-induced vibrations can govern the structural design compared to the effects produced by wind or wave loadings. Therefore, mitigation of the seismic response is a fundamental task to increase structural reliability. This paper proposes redesigning the bottom-fixed offshore wind turbine's traditional transition piece to transform it into a seismic device, through the Reduced Column Section (RCS) approach, recently proposed by the Authors. By adopting an hourglass shape structure of high-strength steel, the novel device allows limiting the maximum stresses within the reduced section, hence protecting the remaining section of the towers and of the monopile. The proposed approach is numerically tested on the 3-dimensional finite element model representing the 15-megawatt reference turbine proposed by the International Energy Agency. Non-linear time history analyses considering the combination of wind and seismic loads are conducted to investigate the seismic reserve capacity factor for abnormal-level earthquakes. Soil-structure interaction effects are captured through direct modelling of the soil-pile system through spring-dashpot systems and site response analysis is conducted to capture the wave propagation within the soil deposit. The novel transition piece is able to protect the wind turbine from collapse by reducing of about 53% of the maximum effective stresses on the tower walls.

Keywords: 15 MW Reference Wind Turbine, Reduced Column Section (RCS), Seismic analysis.

ISSN:2623-3347 © 2023 The Authors. Published by Eccomas Proceedia.
Peer-review under responsibility of the organizing committee of COMPDYN 2023.
doi: 10.7712/120123.10394.20234

1 INTRODUCTION

The worldwide installed capacity of electric power generation from offshore wind sources has developed exponentially over the past decades. It plays an important role for providing renewable energy and towards a low carbon energy supply. Recently, various wind farms have been constructed in different regions, including high seismic active areas such as the coast of Japan, China, the USA, Taiwan, Southern Europe, and India [1, 2]. This highlights that wind turbines in these earthquake-prone areas can be expected to be susceptible to damage under combined multi-hazards loads. Therefore, further studies on seismic performance and assessment methods need to be developed. Remarkably, the seismic design of wind turbines is not directly addressed in current international standards and national codes (e.g., Eurocode 8 [3], IBC [4], IEC 61400-3 [5], ASCE/SEI 7–1043 [6]). These standards and design guidelines suggested considering seismic actions, but their approaches and parameters are mostly employed for building or conventional structures. Moreover, several standards such as DNV-OS-J101 code [7], which is a specific industry code for offshore wind turbines, explicitly states that earthquake resistance should be demonstrated, without addressing all critical aspect that can lead to the wind turbine collapse under extreme conditions.

On the other hand, with the growth in the wind energy industry, larger sizes and rated power have been produced, leading to longer blades and taller towers [8]. Recently, the International Energy Agency (IEA) Wind Technology Collaboration Platform (TCP) Task 37 on systems engineering has developed the IEA Wind 15 MW [9], which is considered in this study. Exhaustive studies on the NREL 5 MW have highlighted the relevance of the seismic response of offshore wind turbines [10-14], however, there are a few studies on the seismic analysis of 15 MW offshore wind turbines. Padrón et al. [8] numerically studied the dynamic and seismic response of the support structures of the NREL 5 MW, IEA Wind 10 MW and IEA 15 MW offshore wind turbines. They have concluded that any earthquakes can generate significant increases in the structural demands of these three wind turbines.

Moreover, the combination with the wind load should be investigated. Rinker et al. [9] compared aeroelastic codes using OpenFAST and HAWC2 of the IEA 15 MW offshore wind turbine. The capabilities and limitations of two different aerodynamic models on capturing the dynamic phenomena of a floating IEA 15 MW turbine were studied by [15]. Furthermore, Niranjan and Ramisetti [16] used OpenFAST to analyse the fully coupled dynamic response of the 15 MW reference turbine mounted over a UMaine VolturnUS-S semi-submersible floating platform. Therefore, the development of recent 15 MW wind turbines should be pursued, and earthquake-induced should be controlled and mitigated for reducing the risk of failure. This study aims to investigate the seismic response of the 15 MW Reference turbine by redesigning the traditional transition piece and offers a novel solution for the vibration control of wind turbines. Nonlinear time history analysis on 3-dimensional finite element models created through the commercial ADINA software [17] is performed. The model is verified through the specialized open-source wind turbine simulation code, OpenFAST [18]. Results will evidence the capability of the novel device to mitigate the seismic response and avoid the tower collapse.

2 THE REDUCED COLUMN SECTION APPROACH

The Reduced Column Section (RCS) approach recently proposed by the Authors in [19] entails the substitution of the traditional transition piece (TP) connecting the pile to the tower (Fig. 1) with an HourGlass Structure (HGS) in order to mitigate the dynamic response of the wind turbines by controlling the shift of the fundamental period and inducing a rocking behavior.

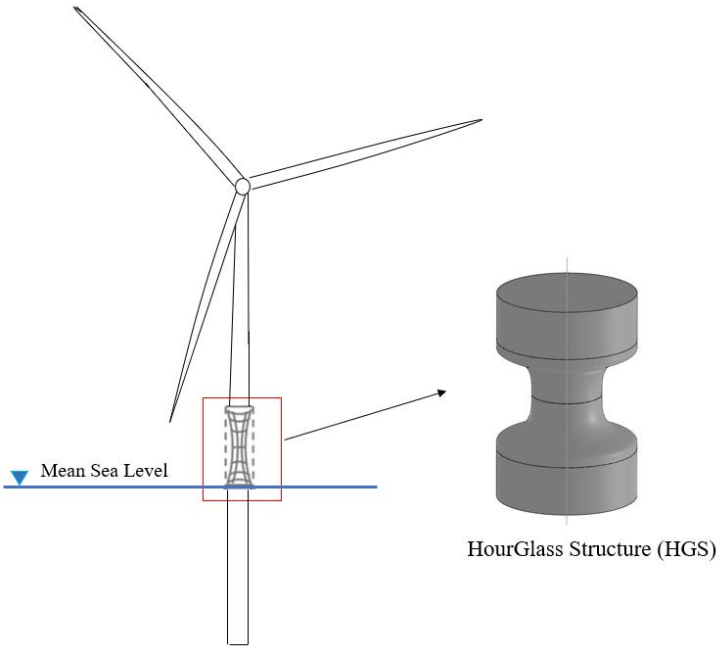

Figure 1: Example of reduced column section approach: the HourGlass Structure (HGS) for offshore WT.

Furthermore, by creating an hourglass shape with reduced cross-sectional diameter, the maximum stresses are limited within the device which acts a mechanical "fuse". Therefore, high-strength steel shall we used to withstand the increment of stresses and improves the moment plastic capacity.

Simplified design for applying the RCS approach is described in [19]. In this study, it will be shown how the controlled development of plastic behaviour can provide an increment of the seismic reserve capacity and mitigation of the maximum stresses on the tower through ductility and energy dissipation.

3 IEA 15 MW REFERENCE OFFSHORE WIND TURBINE

The IEA 15 MW Offshore Reference Wind Turbine (RWT) designed by the National Renewable Energy Laboratory (NREL) and the Technical University of Denmark (DTU), during the International Energy Agency (IEA) Wind Task 37 [20] is considered in this study. It is a 3-bladed upwind tower with 117 m long blades and 240 m rotor diameter. The hub is located about 150 m above the mean sea level (MSL). The tower height is 129.582 m with a varying diameter of 10 m at the base and 6.5 m at the top. The monopile has a length of 75 m with a constant outer diameter of 6 m of which 45 m is embedded in soils, and the remaining 30 m is from the seabed up to the sea level. The pile is connected to the tower through a 15m-high transition piece. Fig. 2(a) shows the front view of the IEA 15 MW turbine model. A summary of the main characteristics is described in Table 1. As described in [20], the soil-foundation behaviour is modeled with a series of spring-dashpot units to represent the soil stiffness profile along the pile length and radiation as well as material damping. The dense sand deposit is characterized by a shear module of 140 MPa, Poisson's ratio of 0.4 and a unit density of 2000 kg/m^3. In this paper, the soil deposit lies on an elastic bedrock characterized by a shear wave velocity of 1000 m/s.

Item	Value
Rated power (MW)	15
Rotor diameter (m)	240
Hub height (m)	150
RNA mass (t)	1017
Blade mass (kg)	65250
Nacelle mass (kg)	646895
Tower mass (t)	860
Tower base and top diameter (m)	10, 6.5
Tower base and top thickness (mm)	41.058, 23.998
Transition piece height (m)	15
Monopile depth (m)	75
Monopile embedment depth (m)	45
Monopile diameter (m)	10
Monopile base and top thickness (mm)	55.341, 45.517

Table 1: Main parameters of the Reference IEA 15 MW RWT.

3.1 Finite Element Model

The reference 15 MW RWT is modelled through the three-dimensional (3D) finite element (FE) software ADINA [17] as shown in Fig. 2(b). The geometrical model consists of three main components, namely, the tower, the transition piece and the monopile. The tower model is divided into 10 segments (1 to 10) with different diameters and lengths (see Fig. 2(a)). Four-node shell elements are used for modelling the steel walls. A mesh convergence study is performed to derive the optimal mesh size for the shell elements of the tower and monopile, and a value of a maximum mesh size of L = 2 m is used for the coarser elements and of L = 0.5 m for the critical areas, such as for the HGS where the maximum stresses are expected.

To account for the inertial coupling of the rotor-nacelle assembly (RNA), a simplified lumped mass approach, depicted in Fig. 3, is used, where the hub and nacelle are modelled as two separated lumped masses. Rigid links are then used to connect them to the top part of the tower. As shown in Fig. 3(b), the nacelle mass (m_N) is located dislocated from the tower axis by a horizontal ($ex_N = 4.720m$) and a vertical offset ($ez_N = 4.275m$). Similarly, the rotor mass (m_R) is eccentric to the axis of the tower by a horizontal and a vertical offset, $ex_R = 12.05m$ and $ez_R = 5.40m$, respectively. The rotor mass, ($m_R = 341825kg$), includes hub and blades masses (see Table 1).

Aerodynamic damping equivalent to 9.6% damping ratio is simulated through a viscous dashpot applied at the nacelle whilst a Rayleigh damping equal to 1.4% is applied to the steel tower and monopile.

The soil-monopile interaction is captured through a series of bi-dimensional plane linearized spring-dashpot systems with 1 spring for each side and direction; their properties are determined and calibrated to match the lateral deformations and frequencies of the linearized spring model with the full-scale 3D soil-pile FE model. A constant stiffness profiles is adopted; the computed horizontal stiffness is equal to 971600000 N/m, and the coefficient of viscosity of the dashpot for the horizontal damping is 17046000 N/ms.

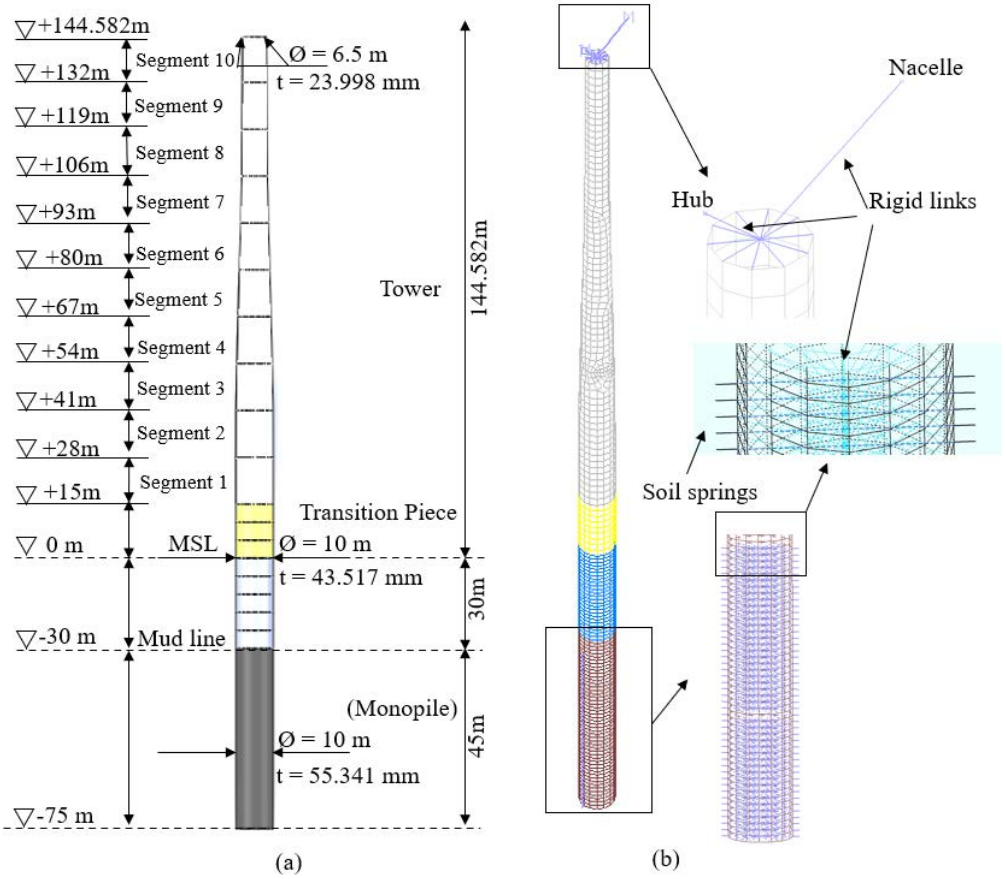

Figure 2: Geometry: (a) the IEA 15-MW reference wind turbine, (b) ADINA model and details.

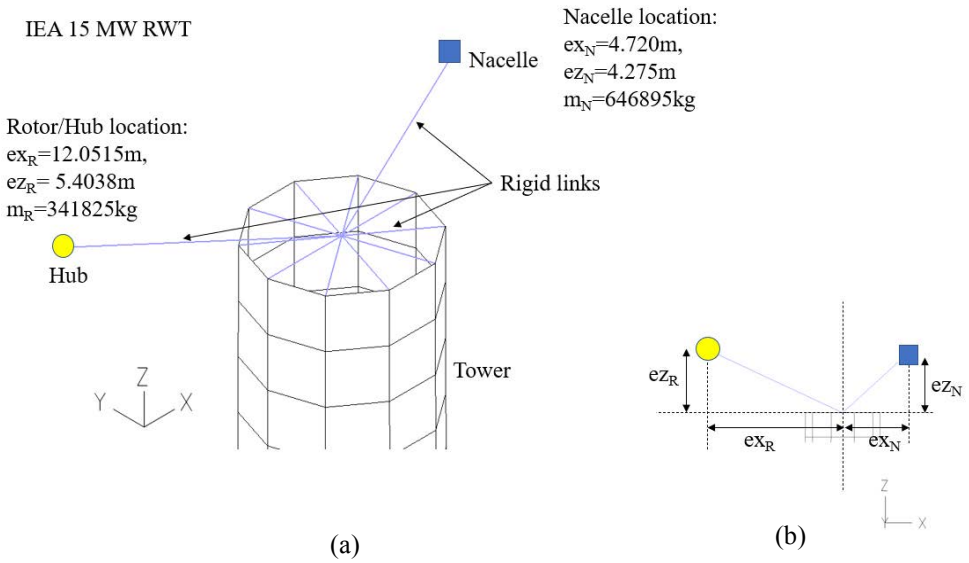

Figure 3: (a) Rotor and nacelle locations, (b) Model of nacelle and rotor with horizontal and vertical eccentricity.

The material properties tower wall and monopile are based on steel S355, however, the density of the S355 is modified to account for paint, secondary steel appurtenances, coatings, and welds. The values of the elastic modulus, density and Poisson's ratio used in this study are 210

GPa, 8600 kg/m^3 and 0.3 respectively. The cyclic plastic behaviour is simulated through the isotropic and kinematic hardening laws characteristics of the Chaboche's model [21]. The isotropic and kinematic hardening parameters of the S355 steel grade are reported in [19].

3.2 Dynamic Loads Modelling

3.2.1 Wind Load

The obtained numerical FE model is first verified through OpenFAST [18], an open-source software package for simulating the coupled dynamic response of wind turbines. The AeroDyn module is used to calculate aerodynamic loadings by using the blade element momentum theory (BEMT). In this study, a steady inflow wind speed of 10 m/s in the fore-aft direction is considered. The aerodynamic forces and moments obtained from OpenFAST are applied as dynamic forces to the hub mass of the 3D finite element model. The structural dynamics responses such as tower displacement and acceleration. Fig. 4 shows the tower displacement at the rotor start-up controlled to maximize the power generation under a steady wind speed of 10 m/s where the static component of the rotor thrust is dominant; the numerical 3D finite element model in ADINA is able to capture sufficiently the structural response under wind load. The approximation of this approach is because of the neglected aerodynamic coupling between wind load and tower simulated in OpenFAST but not in the proposed ADINA FE model.

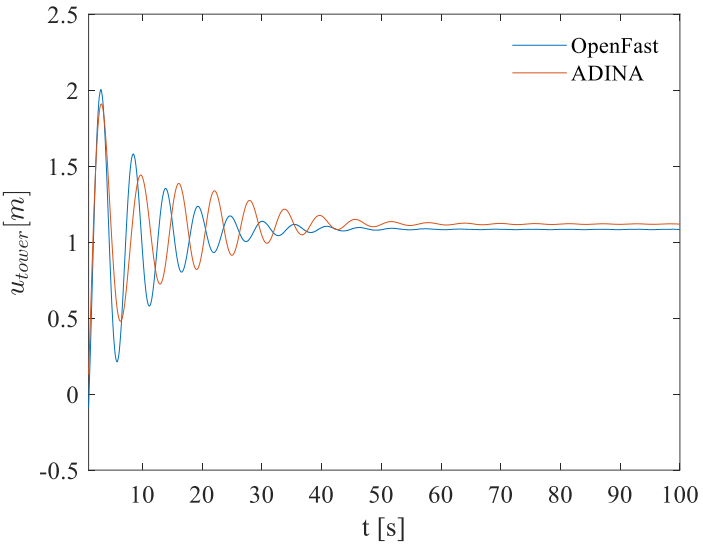

Figure 4: Tower displacements in OpenFast and ADINA under steady wind with rotor speed control.

3.2.2 Seismic Site Response Analysis

The seismic design procedure and criteria are defined according to ISO 19901-2 standard [22] for offshore structures. For an ultimate list state (ULS) design, the structure is designed to suffer little or no damage under the extreme-level earthquake (ELE), which elastic spectrum is defined in ISO 19901-2 [22]. Moreover, the seismic code entails the verification of the abnormal limit state (ALS) for rare earthquakes (ALE); for this scenario, the structure can be subjected to considerable damage without affecting the overall structural integrity, hence avoiding structural collapse or instability. Therefore, structural elements are allowed to develop plastic behaviour.

In this study, Monte Carlo Simulation (MCS) consisting of non-linear time history analyses is carried out to accurately capture the impact of the nonlinearities of the proposed HGS to protect the remaining structural elements of the wind turbine. The horizontal site elastic spectrum of 1000 year return time, $S_{a,site}(T)$ is determined for the site class A where the spectrum value at the fundamental period, $T = 1s$, is $S_{a,site}(T = 1s) = 3.92\, m/s^2$, and at $T = 0.4s$, is $S_{a,site}(T = 0.4s) = 9.81\, m/s^2$.

Acceleration time histories are generated [23] to match on average the corresponding elastic spectrum as shown in Fig. 5(a), where the blue curve represents the target spectrum, and the red curve denotes the elastic spectrum computed by averaging the spectra of 5 generated ground motions (SET 1 – 5). Although accuracy can be improved by increasing the number of generated seismic signals, a relatively good matching is obtained with a few signals, which also are above the prescribed minimum of four sets of time history records established by the ISO 19901 standards.

To correctly model the soil-pile interaction effect, an elastic site response analysis is hence carried out to simulate the propagation of the seismic wave within the soil deposit. By considering the properties of the soil deposit reported, acceleration time histories are obtained at each level where the soil springs are located. The outcropping spectrum is altered by the soil deposit and an amplified spectrum as shown in Fig. 5(a) through a black curve, is obtained at the mud-level surface; Fig. 5(b) shows the time histories at the outcropping bedrock and at the mud level for the selected SET 1 ground motion.

In this study, the seismic action is increased in order to establish the seismic reserve capacity factor, representing the ratio of spectral acceleration causing catastrophic system failure to the ELE spectral acceleration.

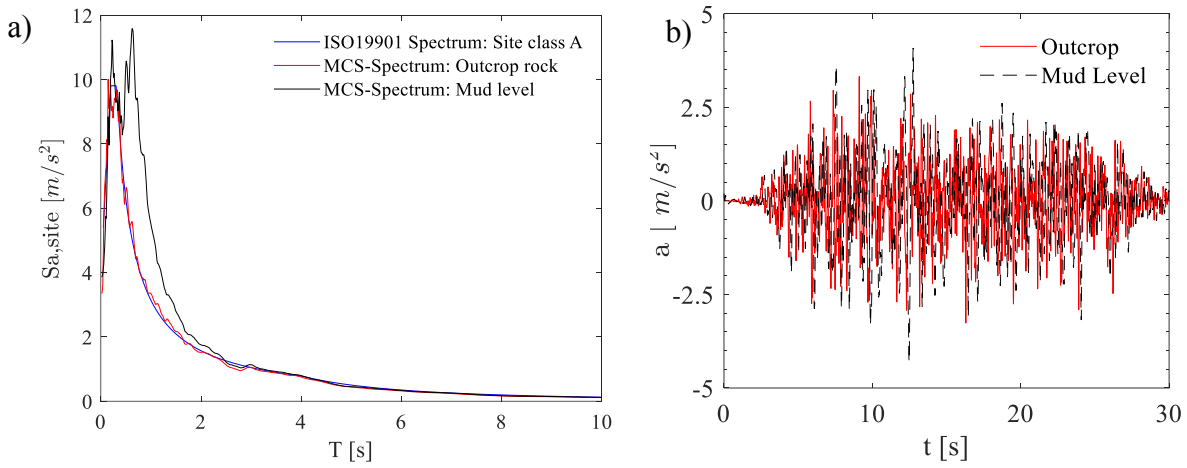

Figure 5: Monte Carlo Simulation of the site Response Analysis: a) Elastic response spectra, b) acceleration time histories of SET 1, at the outcropping bedrock and at the mud level.

3.3 Hourglass Structure

As discussed in section 2, in order to mitigate the dynamic loads induced by the combination of wind and earthquake, an Hourglass structure exploiting the reduced column section approach is used to replace the traditional transition piece. Fig. 6(a) shows the 3D FE models of traditional transition piece (R1) of the Reference IEA 15MW RWT and in Fig.6(b), the developed HGS. The diameter ratio R is defined as the ratio between the outer diameter of RCS and the outer

diameter of the full cross-section of the transition piece. In this case, R is fixed to 0.5 (50% of the original diameter) and the thickness, t, of the HGS wall is tuned to minimize the top tower acceleration. A value of $t = 0.1533\ m$ is obtained.

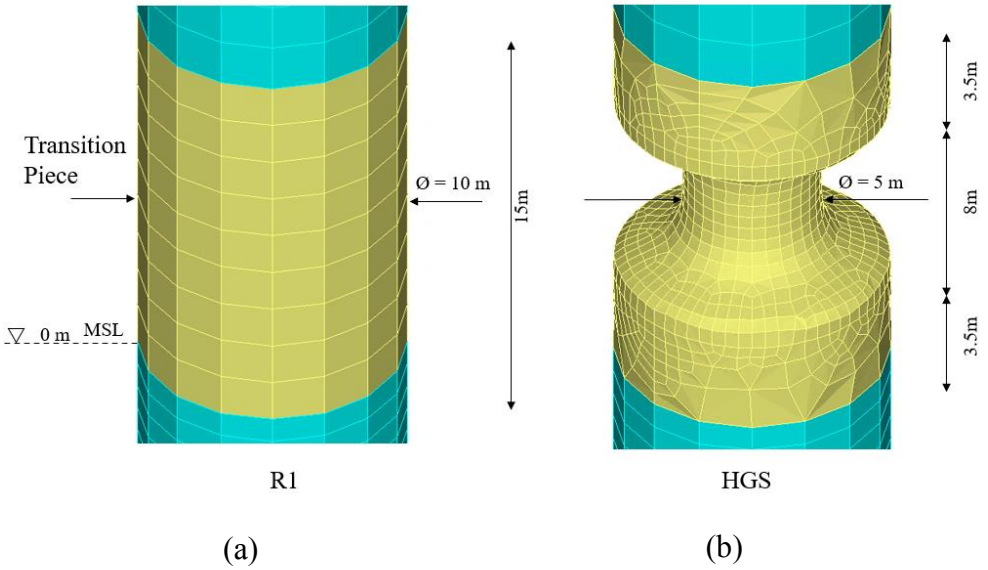

Figure 6: 3D FE model of (a) model R1 (original transition piece), (b) model HGS – Hourglass structure.

3.4. Natural frequency

The natural frequencies of the first two modes of the existing wind turbine (R1) and the modified TP models (HGS) of 15 MW RWT are presented in Table 2. In the design process, the natural frequency should be carefully designed to avoid unplanned resonance effects due to wind turbulence, waves, rotational frequency (P) and blade passing frequencies (2P/3P) [24]. As shown in Table 2, the first mode corresponds to a lower frequency than the rotor frequency (1P) equal to 0.12 Hz, which is called the "soft-stiff" design. It can also be seen that the frequency is reduced for the HGS model due to the smallest cross-section as discussed in Section 2.

Natural frequency	R1 [Hz]	HGS [Hz]
f_1	0.157	0.121
f_2	1.017	0.964

Table 2: Natural frequencies in Hz of R1 and HGS.

4 ANALYSIS AND RESULTS

Nonlinear dynamic time-history analysis of the turbine is performed to assess the efficiency of the proposed HGS in protecting the IEA 15 MW RWT. The numerical analysis process can be divided into three steps:

Step 0 Gravity analysis. A static mass proportional load is applied to determine the initial stresses based on the structural mass of the wind turbine.

Step 1 Wind load analysis. In this step, the aerodynamic loads are applied to the hub level to simulate the transient response of the turbine due to the servo motor.

Step 2 Combined Wind and Seismic analysis. After the stabilization of the transient part of the aerodynamic load, displacement time histories are applied to each spring level to simulate the wave propagation of the seismic input (as explained in Section 3.2.2) considering 5 sets of spectrum-compatible earthquakes.

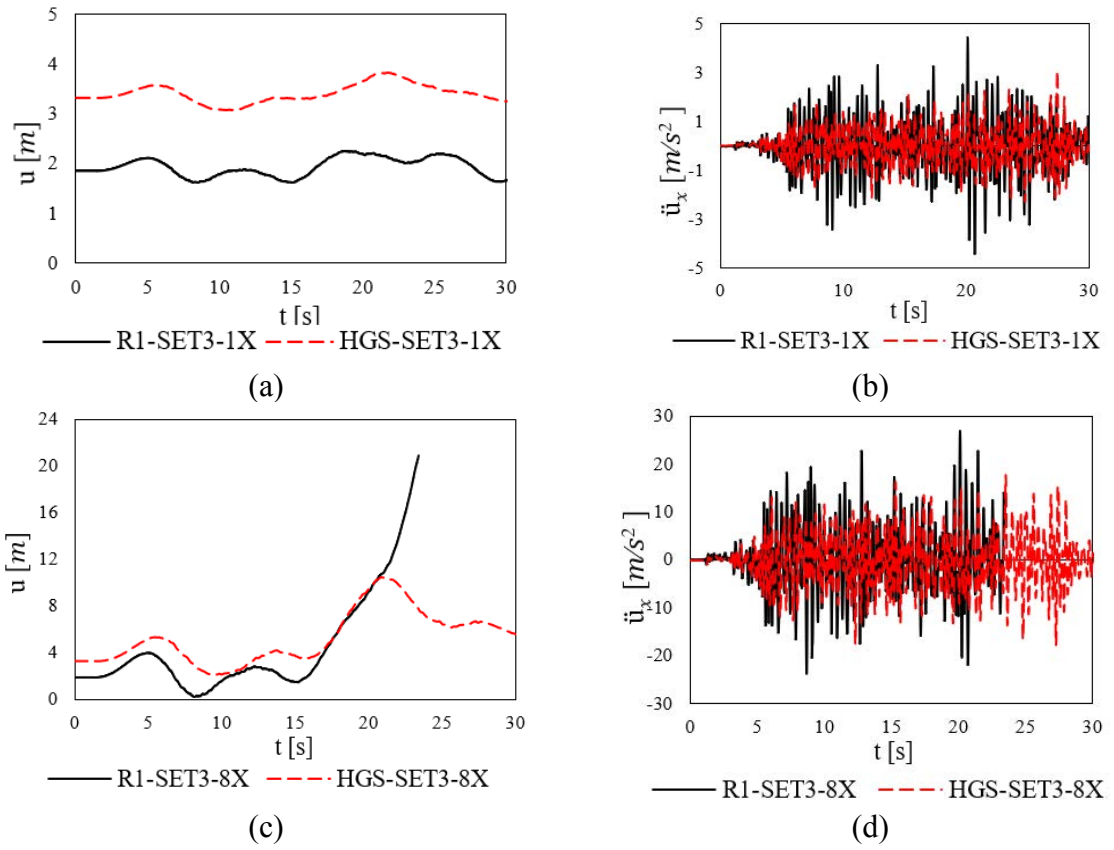

Figure 7: Top displacement (a, c) and acceleration (b, d) time histories of wind turbine for the event EQ set 3.

Segment	1X					
	Average stress (MPa)		Variation	Max Stress (MPa)		Variation
	R1	HGS	(%)	R1	HGS	(%)
10	184.48	181.03	1.87%	214.90	215.03	-0.06%
9	261.76	262.33	-0.22%	314.23	311.51	0.86%
8	272.54	286.83	-5.24%	332.67	326.73	1.78%
7	259.74	275.10	-5.91%	317.75	311.55	1.95%
6	211.80	225.27	-6.36%	249.69	251.65	-0.79%
5	195.24	201.97	-3.45%	217.05	226.37	-4.29%
4	182.47	186.65	-2.29%	198.60	204.95	-3.20%
3	165.82	177.25	-6.89%	174.54	198.16	-13.54%
2	179.11	196.43	-9.67%	186.64	218.23	-16.92%
1	156.39	172.06	-10.02%	162.83	190.51	-17.00%
TP	163.48	541.51	-231.24%	172.16	615.94	-257.77%
Monopile	179.73	189.21	-5.28%	196.89	210.02	-6.67%

Table 3: Results of Comparing Stresses for 1X.

To compute the reserve capacity factor, incremental dynamic analysis is carried out by magnifying the amplitudes of the seismic signal by a factor of 4 and 8 for all the 5 investigated sets. Figs. 7(a) to 7(d) show the displacement and acceleration time histories for a selected set related to the ELE and an abnormal level incremented by 8 times. Whilst for the ELE level, the structural safety is satisfied since no plastic strains are observed, the Reference structure (R1) has collapsed at the considered abnormal level by developing an excessive plastic strain at the top of the tower. The HGS model shows a beneficial reduction of about 33.62% of the maximum acceleration and an average reduction of 11.08%; it is worth noting that compared to the case investigated in [19], the shift in frequency does not have a relevant impact on the structural acceleration. Nevertheless, because of the induced rocking behaviour and "fuse" effect, the HGS is able to avoid the collapse during the abnormal earthquake considered in this study.

Tables 3 to 5 present the results of numerical analyses containing average and maximum effective stresses obtained on the wind tower walls (Segments 1-10) as well as on the transition piece or HGS and on the monopile for every amplification factor (1x-4x-8x). The variation of the maximum stress induced by the HGS is calculated as follows:

$$Variation(\%) = (1 - \left(\frac{V_{HGS}}{V_{R1}}\right)) \times 100 \quad (1)$$

where V_{HGS} and V_{R1} are the values of corresponding average and maximum effective stress, for the HGS model and reference model (R1), respectively. Because of the negligible effect of the shift of the period, a slightly detrimental effect (less than 10% on average) is obtained because of the dominance of the wind load on the seismic effect; also, the HGS behaves linearly, and no dissipation of energy is induced.

By increasing the intensity of the input, beneficial effects are obtained (Table 4) in the upper region of the wind tower where the maximum deformations are occurring. This result is interesting because is opposite to what was obtained in [19] where the higher beneficial effects were obtained nearby the HGS device. For the maximum considered intensity, the R1 model collapses whilst the HGS is able to avoid excessive plastic deformation. Large beneficial effects equal to 44% on average and 53% on the maximum effective stress are obtained.

Segment	4X					
	Average stress (MPa)		Variation	Max Stress (MPa)		Variation
	R1	HGS	(%)	R1	HGS	(%)
10	405.64	399.14	1.60%	430.63	419.12	2.67%
9	454.98	435.80	4.21%	498.73	457.79	8.21%
8	512.27	446.02	12.93%	645.15	468.19	27.43%
7	538.76	438.78	18.56%	673.63	456.37	32.25%
6	427.38	378.43	11.45%	556.49	422.60	24.06%
5	352.24	365.62	-3.80%	388.85	398.17	-2.40%
4	320.88	338.09	-5.36%	356.23	383.49	-7.65%
3	287.12	306.02	-6.58%	311.56	376.85	-20.95%
2	305.01	334.14	-9.55%	345.96	397.12	-14.79%
1	260.83	291.88	-11.90%	301.23	346.96	-15.18%
TP	280.43	879.96	-213.79%	318.92	1053.78	-230.42%
Monopile	328.25	366.79	-11.74%	355.52	399.60	-12.40%

Table 4: Results of Comparing Stresses for 4X.

The distribution of the maximum effective stresses for one selected set is shown in Fig. 8 evidencing the reduction of the stresses at the top of the tower avoiding the collapse of the model. It is worth mentioning that the R1 model collapses for all the 5 considered sets whilst the proposed HGS was able to protect the tower in all the cases.

Finally, the distribution of the plastic strain on the collapsed segments 7-8 are shown on Fig. 9. Although plasticity is triggered in both models, in the reference R1 model the magnitude is higher and occurs at the Side-Side direction of the turbine due to the instability of the segments.

5 CONCLUSIONS

This paper presents an application of the Reduced Column Section approach developed in [19] for the mitigation of the dynamic responses of the IEA 15 MW Offshore Reference Wind Turbine. The Hourglass structure is developed to replace the traditional transition piece. The main conclusions are summarized as follows:

- The HGS was able to mitigate the maximum effective stresses on the tower wall up to 53% compared to the reference structure;
- The HGS avoided the tower collapse when an abnormal level of the earthquake is applied, hence it is able to increase the seismic reserve capacity of the wind turbine;
- The acceleration of the top of the tower is reduced in the case of the HGS model of only about 12.26% because of the high flexibility of the reference structure which is characterized by a low first structural frequency;
- The capability of the HGS of acting as a fuse and because of the induced rocking behaviour allowed to protect the tower from the collapse as instead occurred for the reference wind turbine;
- At low seismic excitation (frequent earthquakes), the wind load is dominant on the structural response and the HGS is providing neither large beneficial nor detrimental effects.

Segment	8X					
	Average stress (MPa)		Variation	Max Stress (MPa)		Variation
	R1*	HGS	(%)	R1*	HGS	(%)
10	511.22	437.83	14.36%	559.44	459.33	17.89%
9	737.38	507.27	31.21%	967.01	522.90	45.93%
8	913.75	509.90	44.20%	1115.98	521.27	53.29%
7	823.99	505.50	38.65%	1036.52	521.57	49.68%
6	677.14	440.92	34.89%	793.47	474.21	40.24%
5	467.22	407.40	12.80%	503.32	429.49	14.67%
4	424.85	393.82	7.30%	436.37	402.75	7.70%
3	408.91	384.27	6.03%	424.05	404.35	4.65%
2	403.60	404.27	-0.16%	412.32	438.80	-6.42%
1	394.90	362.96	8.09%	398.28	392.01	1.58%
TP	368.29	1123.65	-205.10%	378.04	1160.18	-206.89%
Monopile	374.68	424.45	-13.28%	422.77	444.38	-5.11%

(* collapsed tower)

Table 5: Results of Comparing Stresses for 8X.

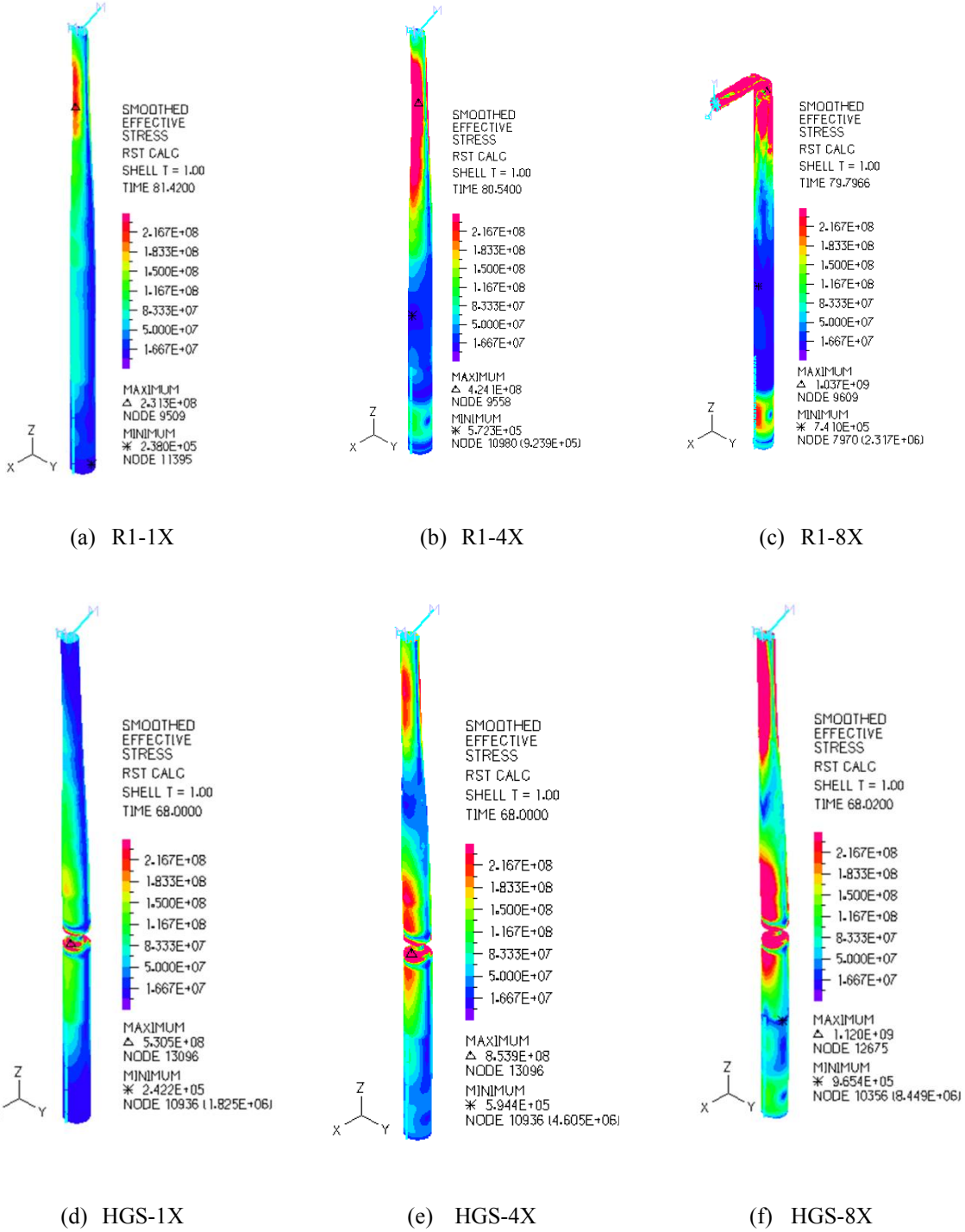

(a) R1-1X (b) R1-4X (c) R1-8X

(d) HGS-1X (e) HGS-4X (f) HGS-8X

Figure 8: Effective stress contour map for: (a-c) R1, (d-f) HGS models.

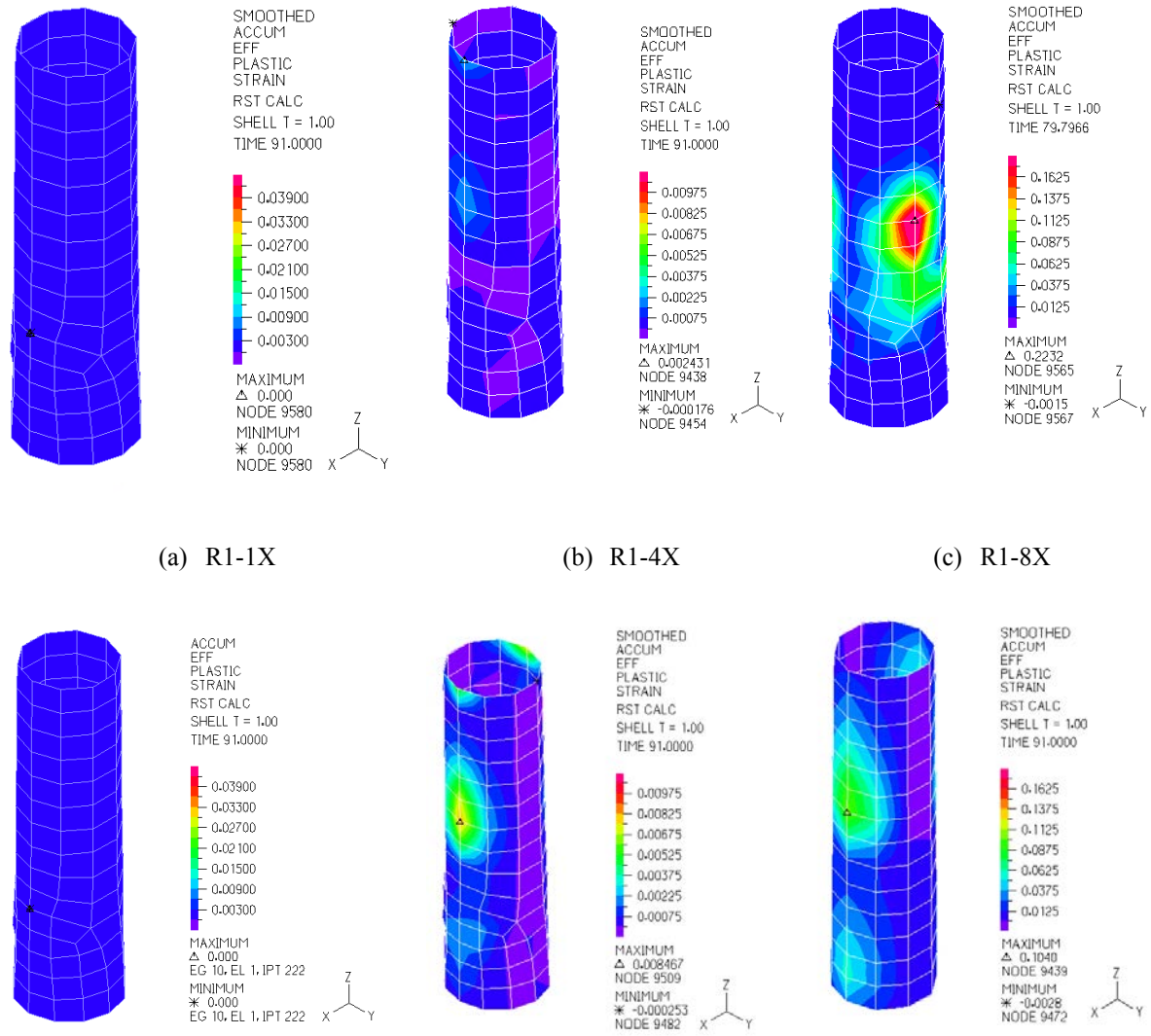

(a) R1-1X (b) R1-4X (c) R1-8X

(d) HGS-1X (e) HGS-4X (f) HGS-8X

Figure 9: Plastic Strain contour map for Segments 7 and 8 for: (a-c) R1, (d-f) HGS models.

6 ACKNOWLEDGEMENT

The authors Tombari and Rostami gratefully acknowledge the financial support of the Engineering and Physical Sciences Research Council (EPSRC) through the New Investigator Award EP/W001071/1 “Structural Life-Cycle Enhancement of Next-Generation Onshore and Offshore Wind Farms”.

REFERENCES

[1] E.I. Katsanos, S. Thöns, and C.T. Georgakis, Wind turbines and seismic hazard: a state‐of‐the‐art review. *Wind Energy*, **19(11)**, pp.2113-2133, 2016.

[2] R. De Risi, S. Bhattacharya, and K. Goda, Seismic performance assessment of monopile-supported offshore wind turbines using unscaled natural earthquake records. *Soil Dynamics and Earthquake Engineering*, **109**, pp.154-172, 2018.

[3] P. Code, Eurocode 8: Design of structures for earthquake resistance-part 1: general rules, seismic actions and rules for buildings. *Brussels: European Committee for Standardization*, 2005.

[4] I. IBC, *International building code (IBC), international code council (ICC). IL*, USA, 2012.

[5] IEC. International Electrotechnical Commission. IEC 61400–3: *wind turbines – Part 3: design requirements for offshore wind turbines. third ed,* 2009.

[6] American Society of Civil Engineers. *Recommended practice for compliance of large 410 land based wind turbine support structures*. Reston, VA: ASCE/AWEA RP2011; 2011.

[7] DNV, Det Norske Veritas. *Design of offshore wind turbine structures. In: Offshore Standard DNV-OS-J101*; 2014. p. 238. Available at: https://www.dnvgl.com/.

[8] L.A. Padrón, S. Carbonari, F. Dezi, M. Morici, J.D. Bordón, and G. Leoni, Seismic response of large offshore wind turbines on monopile foundations including dynamic soil–structure interaction. *Ocean Engineering*, **257**, p.111653, 2022.

[9] Rinker, J., Gaertner, E., Zahle, F., Skrzypiński, W., Abbas, N., Bredmose, H., Barter, G. and Dykes, K., 2020, September. Comparison of loads from HAWC2 and OpenFAST for the IEA Wind 15 MW Reference Wind Turbine. In Journal of Physics: *Conference Series (Vol. 1618, No. 5, p. 052052)*. IOP Publishing.

[10] A. Ali, R. De Risi, A. Sextos, K. Goda, and Z. Chang, Seismic vulnerability of offshore wind turbines to pulse and non‐pulse records. *Earthquake Engineering & Structural Dynamics*, **49(1)**, pp.24-50, 2020.

[11] S. Bhattacharya, S. Biswal, M. Aleem, S. Amani, A. Prabhakaran, G. Prakhya, D. Lombardi, and H.K. Mistry, Seismic design of offshore wind turbines: good, bad and unknowns. *Energies*, **14(12)**, p.3496, 2021.

[12] V. Chaudhari, S.N. Somala, Seismic performance of offshore wind turbine in the vicinity of seamount subduction zone. *Structures*, 34:423–32, 2021. https://doi.org/10.1016/j.istruc.2021.07.080.

[13] A.M. Kaynia, Seismic considerations in design of offshore wind turbines. *Soil Dynamics and Earthquake Engineering*, 124:399–407, 2019. https://doi.org/10.1016/j.soildyn.2018.04.038.

[14] H.A.C. Filho, S.M. Avila, J.L. de Brito, Dynamic analysis of onshore wind turbines including soil–structure interaction. *J Braz Soc Mech Sci Eng,* 43:143, 2021. https://doi.org/10.1007/s40430-021-02837-5.

[15] N. Ramos‐García, S. Kontos, A. Pegalajar‐Jurado, S. González Horcas, and H. Bredmose, Investigation of the floating IEA Wind 15 MW RWT using vortex methods Part I: Flow regimes and wake recovery. *Wind Energy*, **25(3)**, pp.468-504, 2022.

[16] R. Niranjan, and S.B. Ramisetti, Insights from detailed numerical investigation of 15 MW offshore semi-submersible wind turbine using aero-hydro-servo-elastic code, *Ocean Engineering*, **251**, p.111024, 2022.

[17] ADINA. Watertown. *MA: ADINA R&D*, Inc; 2021.

[18] OpenFAST Documentation, 2022. Release v3.2.0. National Renewable Energy Laboratory, https://raf-openfast.readthedocs.io/en/docs-turbsim/index.html Code published at https://github.com/IEAWindTask37/IEA-15-240-RWT.

[19] R. Rostami, A. Tombari, A novel reduced column section approach for the seismic protection of wind turbines. *Engineering Structures*, **282**, p.115807, 2023. https://doi.org/10.1016/j.engstruct.2023.115807.

[20] E. Gaertner, J., Rinker, L., Sethuraman, F., Zahle, B., Anderson, G.E., Barter, N.J., Abbas, F., Meng, P., Bortolotti, W. Skrzypinski, and G.N., Scott, IEA wind TCP task 37: definition of the IEA 15-megawatt offshore reference wind turbine (No. NREL/TP-5000-75698), 2020. *National Renewable Energy Lab. (NREL)*, Golden, CO (United States).

[21] J.L. Chaboche, Time-independent constitutive theories for cyclic plasticity. *International Journal of plasticity*, 2(2), pp.149-188, 1986.

[22] ISO 19901-2, 2007. International organization for standardization. ISO 19901-2:2017 petroleum and natural gas industries — Specific requirements for offshore structures — Part 2: Seismic design procedures and criteria.

[23] M. Shinozuka, G. Deodatis, G., Simulation of Stochastic Processes by Spectral Representation. *Applied Mechanics Reviews*, **44**, 191–204, 1991. https://doi.org/10.1115/1.3119501.

[24] L. Arany, S. Bhattacharya, S. Adhikari, S.J. Hogan, and J.H.G. Macdonald, An analytical model to predict the natural frequency of offshore wind turbines on three-spring flexible foundations using two different beam models. *Soil Dynamics and Earthquake Engineering*, **74**, pp.40-45, 2015.